Numerical and Experimental Investigation of Grounding Electrode Impulse-Current Dispersal Regularity Considering the Transient Ionization Phenomenon

Jingli Li, *Member, IEEE*, Tao Yuan, Qing Yang, *Member, IEEE*, Wenxia Sima, Caixin Sun, and Markus Zahn, *Life Fellow, IEEE*

***Abstract*—This paper presents a numerical method, combined the finite element method in the spatial domain with the finite difference time domain, to calculate the transient impulse response of grounding systems considering the ionization phenomenon. In this numerical method, space-time variable soil resistivity is used to simulate the soil ionization phenomenon where soil resistivity is controlled according to its relationship with the local instantaneous value of the electric field and no a priori hypothesis on the geometrical shape of the ionized region around the electrodes is necessary. Based on the widely accepted principle of dimensional similarity, this paper makes simulated experimental investigations on the impulse-current dispersal regularity of grounding electrodes with various structures. The proposed numerical scheme is validated by comparing computed results with experimental results and simulation results in literature. Based on the measurement and simulation results, the impulse response regularity of grounding electrodes is discussed and the effect of ionization on human and installations safety is reported.**

***Index Terms*—Electrodes, electromagnetic fields, finite difference methods, finite-element methods, grounding, impulse testing, ionization, lightning protection, nonlinear equations, numerical analysis, soil.**

I. Introduction

GROUNDING systems are important part of the power system that protect power lines and power apparatus from severe ground faults and lightning currents. The grounding systems should have "sufficiently low impedance and current-carrying capacity to prevent the buildup of voltages that may result in undue hazard to connected equipments and to persons" [1]. In order to obtain the best design of an electrical system that can protect power system installations against anomalous events, it is useful to analyze the behavior of grounding systems when they are excited by impulse currents. In particular, the accurate simulation of the nonlinear transient behavior of the soil, the analysis of the current density distribution in the soil surrounding the grounding electrodes, and a study on how to apply the local electromagnetic field and current density distribution regularity to the design of the grounding system for the best high frequency and dynamic performance becomes a fundamental task in power system.

There are numerous studies on the performance of grounding systems, and several models are proposed to analyze and predict the impulse characteristic of a grounding system based on circuit or electromagnetic field approaches [2]–[12]. However, when a grounding system is subjected to high current discharge, the complex dynamic and nonlinear ionization phenomenon in the soil surrounding the electrodes is often omitted or simplified through the enlargement of the conductor radius [2]–[9].

To analyze the electromagnetic field and current density distribution regularity in the soil and to optimize the shape and dimensions of the grounding system, a program code that can simulate the evolution of the soil ionization phenomenon is necessary. Moreover, experimental and theoretical studies on the ionization phenomenon show that the nonlinear ionization processes of the soil surrounding the electrode is time and space varying and that the soil ionization zone around the grounding conductor is not uniform. Hence, this work aims to calculate the impulse characteristic of grounding systems by the method that combines finite element analysis in the spatial domain with finite difference analysis in the time domain. The time and space variable soil resistivity controlled by the electric field intensity of every finite soil element for every time step is introduced to simulate the time varying ionization process.

Several impulse experiments have been performed on full scale grounding grids or on corresponding physical grounding models in electrolytic tanks or sand ponds [13]–[17]. An investigation of grounding grid impulse characteristics is described in [13], where only the impulse current and the impulse voltage at the injection point were measured, and the results are related to cases without soil ionization around the grounding conductor because of the relatively small current impulse amplitude. The impulse current distribution of a long grounding rod was studied

Manuscript received December 20, 2010; revised April 06, 2011; accepted May 25, 2011. Date of publication August 30, 2011; date of current version October 07, 2011. This work was supported in part by the National Basic Research Program of China (973 Program) (2009CB724504), in part by the National Natural Science Foundation of China (50707036), and in part by the National 111 Project of China (B08036). Paper no. TPWRD-00974-2010.

J. L. Li, T. Yuan, Q. Yang, W. X. Sima, and C. X. Sun are with the State Key Laboratory of Power Transmission Equipment and System Safety and New Technology, Chongqing University, Chongqing 400044, China (e-mail: lijingli1022@yahoo.com.cn).

M. Zahn is with the Department of Electrical Engineering and Computer Science, Research Laboratory of Electronics, Laboratory for Electromagnetic and Electronic Systems, High Voltage Research Laboratory, Massachusetts Institute of Technology, Cambridge, MA 02139 USA (e-mail: zahn@mit.edu)

Color versions of one or more of the figures in this paper are available online at http://ieeexplore.ieee.org.

Digital Object Identifier 10.1109/TPWRD.2011.2158860

in [17]. In its full scale experiment, the grounding rod was divided into sections when current was measured by a current divider. The division may be change the impulse current distribution of the grounding rod and probably cause errors. To avoid human hazards and to protect the interconnected electrical and electronic equipment and installations, it is necessary to find a more accurate impulse current dispersal regularity of grounding electrodes, as well as a more suitable configuration of grounding system with more sufficient current-carrying capacity.

Based on the principle of dimensional similarity [18], this paper makes simulation experimental investigations on the impulse current dispersal regularity of grounding electrodes with various structures at the Grounding Technology Laboratory of Chongqing University. The results of the proposed grounding system simulation model are validated through measurement comparisons. The impulse current dispersal regularity of grounding electrodes and the soil ionization process are investigated in detail based on measurement and simulation computation results.

II. Soil Ionization

To simulate the time-varying soil ionization process under high impulse current, the physical process of the impulse current leakage into the soil through the grounding system is studied. The space-time variable soil resistivity approach is then used to simulate the ionization phenomenon in the soil.

A. Transient Soil Ionization Process

When a current is discharged into the soil through a ground electrode, the spatial electrical field E is generated within the soil in accordance with the constitutive equation:

$$\boldsymbol{E} = \rho \boldsymbol{J} \tag{1}$$

where ρ is the soil resistivity and $\boldsymbol{J}$ is the current density at the point under consideration.

The experiment to quantitatively research nonlinear characteristics of soil resistivity was adopted in [19]. In this experiment, the soil sample was putted in the square measuring electrode; then regulated the voltage putted on the measuring electrode and measured the current and voltage value in the soil sample. So resistance R of soil sample was obtained by using Ohm law $\mathrm{R} = \mathrm{U}/\mathrm{I}$. According to the relationship of resistance and resistivity, we could get the soil sample resistivity, and according to the relationship of voltage and electric field strength, we could get the electric field strength in the soil sample.

The experiment found that the soil resistivity declines continuously with increasing electric field strength when the electric field strength exceeds a certain value but does not reach the ionization field strength $\boldsymbol{E}_{\mathrm{c}}$. In [19, Fig.1.2.6], obtained from the soil nonlinear characteristic experimental, the relationship between them at the different soil initial resistivity ρ_0 is presented. This phenomenon illustrates the nonlinear conduction characteristic of soil.

With the increasing injected current, wherever $\boldsymbol{E}$ exceeds $\boldsymbol{E}_{\mathrm{c}}$, soil ionization occurs. In 1985, M. Loboda observed a 10% to 30% voltage drop in the ionization region of different kinds of soil in a coaxial cylindrical experimental setup [20]. So resistivity in the ionization region cannot be the same as that in the metal of the grounding electrodes. A thorough analysis of experimental results from the literature and from experiments conducted in the high voltage laboratory of the authors show that the ionization region of soil retains some percentage of the original or preionization soil resistivity. For different types of electrodes, different soil resistivities ranging from $50\ \Omega \cdot \mathrm{m}$ to $827\ \Omega \cdot \mathrm{m}$, and different values of injection currents ranging form several amperes to several thousand amperes, the residual resistivity in the ionization region varied in a range from 1.7%to 47% of the original soil resistivity with very large scatter. However, the distribution is approximately log-normal with geometric mean of 6.77%, and the medium value of 6.6%. A typical residual resistivity in ionization region of 7% might be chosen to model the effect of soil ionization [21].

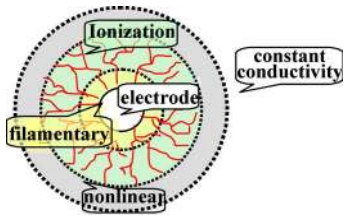

Fig. 1. Spark discharge domain around electrode.

A. C. Liew observed that at a higher lightning current, discrete filamentary arc paths appear in the high-resistivity wet loamy sand in the presence of rain sprays [12]. To simulate heavy rain, water sprays were directed to wet loamy sand when the current impulses were applied, and very spectacular surface flashovers were observed.

In words, according to the value of spatial electric field $\boldsymbol{E}$, soil can be classified as four portions, e.g., filamentary region, ionization region, nonlinear region and constant conductivity region outside the nonlinear region, as shown in Fig. 1.

The soil is not a homogenous and isotropic medium mainly because of variations in water content and grain size. Consequently, current becomes concentrated along a series of discrete channels, and in contrast to what has been assumed by previous models, the ionized zone does not show uniform shapes along the grounding electrode. This was also observed in laboratory [22]. The discrete breakdown channels and the nonuniform ionization region in soil were observed in indoor experiments and recorded on X-ray sensitive films [23].

The ionized region of soil around the grounding electrodes is not well shaped (or not uniform as previously known), and the resistivity of the soil surrounding the conductor is a varying function of electrical field intensity in the soil. Therefore, the previously utilized approach, in which the ionization is omitted or simplified through the enlargement of the conductor radius, does not suitable for the transient analysis of electromagnetic field and current density distribution in the soil which is the basis of optimization design of grounding system. The use of a space-time variable soil resistivity function is chose to simulate the real physical phenomena.

B. Soil Ionization Model

To simulate the time varying ionization process and the nonuniform ionized zone, the space-time variable resistivity

approach can be usefully employed. According to the spatial electric field $\boldsymbol{E}$ obtained from the numerical scheme which incorporated FEM with FDTD, the space-time varying resistivity function of soil is introduced as follow:

If the electric field $\boldsymbol{E}$ of any local node in the soil element fulfills the condition $\boldsymbol{E} < \boldsymbol{E}_{\rm c}$, the soil nonlinear phenomenon begins in the local node and the resistivity of this node is obtained according to the relationship between ρ and the electric field strength $\boldsymbol{E}$

$$\rho = \rho_0 f(\boldsymbol{E}) \tag{2}$$

where $\boldsymbol{E}_{\rm c}$ is the soil ionization gradient, according to the theoretical analysis in [22], the value of $\boldsymbol{E}_{\rm c}$ is set equal to that suggested by Mousa, $\boldsymbol{E}_{\rm c} = 300{\rm kV/m}$, ρ_0 is the soil original resistivity and $\rho = \rho_0 f(\boldsymbol{E}) = 0.4121^{E}$ is the nonlinear function relationship between ρ and $\boldsymbol{E}$ obtained from the experimental results in [19].

If the electric field $\boldsymbol{E}$ of any local node in the soil element fulfills the condition $\boldsymbol{E}_{\rm c} < \boldsymbol{E} < \boldsymbol{E}_{\rm s}$, the breakdown caused by ionization occurs in the local node. According to the analysis of experimental results, a typical percentage of residual resistivity in the ionization region versus soil resistivity (7%) can be chosen to model the effect of soil ionization [21]

$$\rho = 7\%\rho_0. \tag{3}$$

In the same manner, when the electric field $\boldsymbol{E}$ of any local node in the soil elements fulfills the condition $\boldsymbol{E}_{\rm s} < \boldsymbol{E}$, breakdown by sparking occurs and soil resistivity is equal to the grounding conductor resistivity $\rho_{\rm c}$

$$\rho = \rho_{\rm c}. \tag{4}$$

Here, we define $\boldsymbol{E}_{\rm s} = \alpha \boldsymbol{E}_{\rm c}$, the coefficient $\alpha \geq 1$ depends on the transient current I (i.e., as the current rise and penetrate into the earth, the larger the injected current I, the coefficient α and $\boldsymbol{E}_{\rm s}$ will be smaller). A smaller $\boldsymbol{E}_{\rm s}$ means a larger sparking area. In other words, the higher the injected current is, the larger the sparking area is. The relationship equation of I and α can be obtained from the literature [12].

As shown in Fig. 2, the proposed model can simulate the diffuse growth of increasing ionization and the filamentary arc paths. These effects are dominant at the highest value of the surge current and particularly at high soil resistivity. In this paper, the numerical method based on electromagnetic field theory can compute the spatial electric field at every time step, hence, the instantaneous geometries of the ionized region are automatically built according to the actual spatial electric field at every time step. No predefined location and shape of soil ionized zones need to be introduced.

III. Transient Analysis Model of the Grounding System

A. Numerical Model of the Grounding System

The electromagnetic field caused by the surge current flowing through the grounding system into the soil is time varying. Moreover, the ratio of the absolute value of conduction current density $\boldsymbol{J}_{\rm c}$ to the absolute value of displacement current density $\boldsymbol{J}_{\rm d}$ is equal to $1/(\omega\rho\varepsilon)$. The ratio indicates that the displacement current cannot be ignored especially for soil with high resistivity. Using the quasi-static Maxwell's equations, the dissipation process of impulse current can be described by

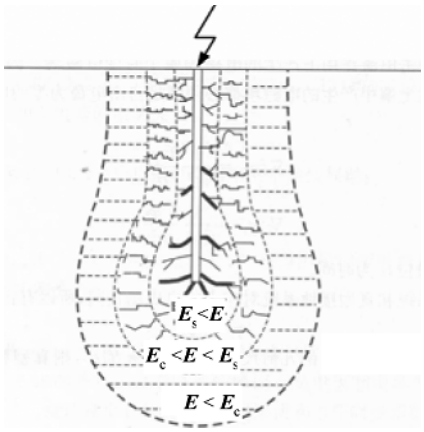

Fig. 2. Space variable soil resistivity model under impulse current.

$$\nabla \times \boldsymbol{H} = \boldsymbol{J}_{\rm c} + \frac{\partial \boldsymbol{D}}{\partial t} \tag{5}$$

$$\nabla \times \mathbf{E} = 0 \tag{6}$$

$$\nabla \cdot J = 0 \tag{7}$$

where $\boldsymbol{H}$ is the magnetic field intensity, $\boldsymbol{D}$ is the electric flux density, $\boldsymbol{E}$ is the electric field intensity, and $\boldsymbol{J}$ is the total current density, which includes conduction and displacement currents.

The field quantities also satisfy the following constitutive equations:

$$\boldsymbol{H} = \frac{1}{\mu}\boldsymbol{B} \tag{8}$$

$$\boldsymbol{J} = \left(\gamma + \varepsilon\frac{\partial}{\partial t}\right)\boldsymbol{E} \tag{9}$$

$$\boldsymbol{D} = \varepsilon \boldsymbol{E} \tag{10}$$

where $\mu, \gamma = 1/\rho$, and ε are the magnetic permeability, conductivity, and the permittivity of the material under consideration. The coefficient $\gamma + \varepsilon\partial/\partial t$ is the general conductivity; it is equivalent to $\gamma + j\omega\varepsilon$ in the frequency domain.

Using the electric scalar potential φ ($\varphi\boldsymbol{E} = -\nabla\varphi$), the transient electromagnetic field is described by Laplace's equation and boundary conditions

$$\varepsilon\frac{\partial}{\partial t}(\nabla^2\varphi) + \nabla\cdot(\gamma\nabla\varphi) = 0. \tag{11}$$

At infinity

$$\varphi = 0. \tag{12}$$

On the earth's surface

$$\left(\gamma + \varepsilon\frac{\partial}{\partial t}\right)[\vec{\boldsymbol{n}}\cdot(\nabla\varphi)] = 0. \tag{13}$$

On the injected surface

$$\int_s -\left(\varepsilon\frac{\partial}{\partial t} + \gamma\right)\nabla\varphi\cdot\vec{\boldsymbol{n}}ds = I \tag{14}$$

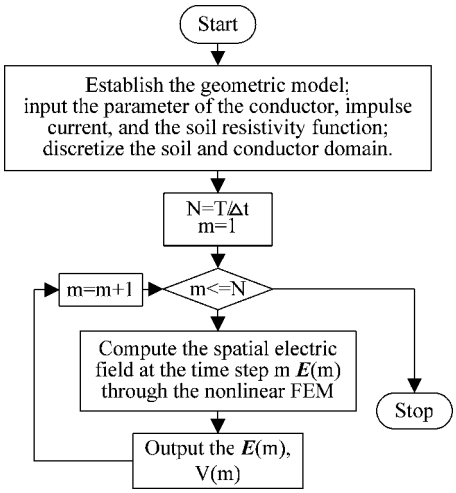

Fig. 3. Flow chart of the numerical model.

where $\vec{\boldsymbol{n}}$ represents unit normal vector of the element surface.

Laplace's (11) is the partial differential equation of the voltage field dependent on time and spatial coordinates. The study requires FEM in the spatial domain, incorporated with FDTD in the time domain. Fig. 3 presents the flowchart of the numerical model. The following two sections introduce the FEM and the FDTD in detail.

B. FEM Formulation in the Spatial Domain

The ten-node tetrahedron element developed from the four-node tetrahedron element is more suitable for the complex domain. It is chosen to discretize the soil and the grounding system domains. Subsequently, the potential φ^e of an arbitrary element is expanded by nodal basis functions

$$\varphi^e = \sum_{j=1}^{10} N_j^e \varphi_j^e \tag{15}$$

where N_j^e is the second-order polynomial nodal shape function of node j in the element e, and φ_j^e is the voltage value of the node j in the element e.

By applying the Galerkin formulation of FEM and the additional transformation of the "semi-infinite space" [24], equations of the 3-D finite element in the soil region and the conductors are obtained. Equations of the 3-D finite element in the nontransformed domain are:

$$R_{\mathrm{i}}^{\mathrm{e}} = \int_{V^{\mathrm{e}}} N_{\mathrm{i}}^{\mathrm{e}} \left[\varepsilon \frac{\partial}{\partial t} (\nabla^2 \varphi^{\mathrm{e}}) + \nabla \cdot (\gamma \nabla \varphi^{\mathrm{e}}) \right] dV = 0 \quad (i = 1, 2 \cdots 10) \tag{16}$$

where V_{e} is the integral domain volume of finite element e.

Since soil conductivity γ is a time-space function that varies with the electric field $\boldsymbol{E}$, according to Green's formula, (16) can be translated to

$$R_{\mathrm{i}}^{\mathrm{e}} = \int_{V^{\mathrm{e}}} \left[\left(\varepsilon \frac{\partial}{\partial t} + \gamma \right) \nabla N_{\mathrm{i}}^{\mathrm{e}} \cdot \nabla \varphi^{\mathrm{e}} \right] dV - \int_{\partial V^{\mathrm{e}}} \left(\varepsilon \frac{\partial}{\partial t} + \gamma \right) \times N_{\mathrm{i}}^{\mathrm{e}} (\vec{\boldsymbol{n}} \cdot \nabla \varphi^{\mathrm{e}}) ds = 0 \ (i = 1, 2 \cdots 10) \tag{17}$$

where ∂V^e is the boundary of the tetrahedron element.

The substitution of (15) into (17) results in the following Galerkin residual equations of an element:

$$R_{\mathrm{i}}^{\mathrm{e}} = \sum_{j=1}^{10} \varphi_{\mathrm{j}}^{\mathrm{e}} \int_{V^{\mathrm{e}}} \left[\left(\varepsilon \frac{\partial}{\partial t} + \gamma \right) \nabla N_{\mathrm{i}}^{\mathrm{e}} \cdot \nabla N_{\mathrm{j}}^{\mathrm{e}} \right] dV = 0 \quad (i = 1, 2, \ldots 10). \tag{18}$$

Particularly, the equations of the 3-D finite elements that are linked with the injected surface are obtained as

$$R_{\mathrm{i}}^{\mathrm{e}} = \sum_{j=1}^{10} \varphi_{\mathrm{j}}^{\mathrm{e}} \int_{V^{\mathrm{e}}} \left[\left(\varepsilon \frac{\partial}{\partial t} + \gamma \right) \nabla N_{\mathrm{i}}^{\mathrm{e}} \ldots \nabla N_{\mathrm{j}}^{\mathrm{e}} \right] dV - \int_{\partial V^{\mathrm{e}}} N_{\mathrm{i}}^{\mathrm{e}} \sigma ds = 0 \ (i = 1, 2, \ldots 10) \tag{19}$$

where $\boldsymbol{\sigma} = (\varepsilon \partial / \partial t + \gamma) \nabla \varphi$ is the normal current density on the injected surface. The surface integral in ∂V^e is kept to prescribe a current source in a given surface as a nonhomogeneous boundary condition.

In the transformed domain, the equations of the 3-D finite element are

$$R_i^e = \sum_{j=1}^{10} \phi_j^e \int_{V^e} \left[(\nabla' N_i^e)^T \, \mathrm{T}^T \left(\gamma + \varepsilon \frac{\partial}{\partial t} \right) \mathrm{T} |\mathrm{T}^{-1}| \nabla' N_j^e \right] dV' = 0 \ (i = 1, 2 \cdots 10) \tag{20}$$

where ∇' is the Del operator in transformed coordinate space and $\mathrm{T} = (\partial x_i' / \partial_j)$ is the Jacobian matrix of the spatial transformation T [24].

By integral operation in the spatial domain, finite element equations at time t (18)–(20) lead to the following algebraic equation:

$$[K]_t \{\varphi\}_t + [N] \left\{ \frac{\partial \varphi}{\partial t} \right\}_t = \{P\}_t \tag{21}$$

where $[\mathrm{K}]_\mathrm{t}$ is the total stiffness matrices at time t, [N] is the transient matrices, $\{\varphi\}$ is the potential in the soil and the conductors at time t, and $\{P\}$ is the load vector at time t which represents the impulse current source.

It is worth noting that (21) is a differential equation of the voltage as a function of time. Moreover, the total stiffness matrices $[\mathrm{K}]_\mathrm{t}$ are controlled by the electric field at time t, so the finite element (21) is a nonlinear equation. The FDTD method used to overcome this problem is introduced in the next section.

C. Finite Difference Formulation in the Time Domain

The transient voltage (21) obtained from (11) by the Galerkin formulation of the FEM is a nonlinear equation. In the calculations, we apply the finite difference in the time domain.

1) Initial Conditions: To solve (11), initial conditions, as well as boundary conditions, are required. In actual engineering,

when there is no impulse current dissipated into the soil through the grounding electrodes, the voltage field in the soil and the grounding conductors is equal to zero

$$\{\varphi\}_0 = (\varphi_1\ \varphi_2 \cdots \varphi_{\mathrm{n}})_0^T = 0 \tag{22}$$

where the voltages $\{\varphi\}_0$ represents the initial voltage field in the soil and in the conductors.

2) Difference Scheme: To calculate the differential equation in the time domain, we introduce the two-point finite difference scheme

$$\beta\left\{\frac{\partial\varphi}{\partial t}\right\}_t + (1-\beta)\left\{\frac{\partial\varphi}{\partial t}\right\}_{t-\Delta\mathrm{t}} = \frac{1}{\Delta t}\left(\{\varphi\}_t - \{\varphi\}_{t-\Delta\mathrm{t}}\right) + O(\Delta t) \tag{23}$$

where $O(\Delta t)$ represents truncation errors, Δt is the time step, and β fulfills the condition$0 \le \beta \le 1$. when $\beta = 2/3$, the Galerkin difference scheme is obtained as follows:

$$\frac{2}{3}\left\{\frac{\partial\varphi}{\partial t}\right\}_t + \frac{1}{3}\left\{\frac{\partial\varphi}{\partial t}\right\}_{t-\Delta t} = \frac{1}{\Delta t}\left(\{\varphi\}_t - \{\varphi\}_{t-\Delta t}\right) + O(\Delta t). \tag{24}$$

The Galerkin difference scheme has higher accuracy and has unconditional stability. This paper applies this difference format.

3) Calculation Formulation of the Transient Potential: By combining (21), a spatial finite element equation at any discrete time, with the time difference (24), and ignoring truncation errors, we can obtain the calculation formulation of the transient potential field

$$\begin{aligned}\{\varphi\}_t = {} & \frac{\Delta t}{3}\left([E] + \frac{2\Delta t}{3}[N]^{-1}[K]_t\right)^{-1} \\ & \times [N]^{-1}\left(2\{p\}_t + \{p\}_{t-\Delta t}\right) \\ & + \left([E] + \frac{2\Delta t}{3}[N]^{-1}[K]_t\right)^{-1} \\ & \times \left([E] - \frac{\Delta t}{3}[N]^{-1}[K]_{t-\Delta t}\right)\{\varphi\}_{t-\Delta t}\end{aligned} \tag{25}$$

where [E] is the n^*n unit matrix.

For the given soil and conductor structure (the total stiffness matrix [K] and the unsteady matrix are fixed), according to the initial conditions and the boundary load vectors $\{\mathrm{P}\}_{\mathrm{t}}$, the voltage field $\{\varphi\}_t$ can be obtained through (25). Based on $\boldsymbol{E} = -\nabla\varphi$ and $\boldsymbol{J} = \gamma\boldsymbol{E}$, the transient electric field and the transient current field distribution in the domain of soil and the conductors can be obtained.

The total stiffness matrix [K] is a function of electric field E. Equation (25) is a nonlinear equation due to the nonlinear characteristic, ionization phenomenon, and the sparking phenomenon of the soil surrounding the grounding electrodes.

IV. Experimental Scheme

To verify the reliability of the program solution, based on the principle of dimensional similarity [18], we make simulation experimental investigations on the impulse-current distribution of grounding electrodes at the Grounding Technology Laboratory of Chongqing University.

The simulation experiment is performed on grounding device models with smaller scaled geometric dimensions. If the geometrical dimensional scale between the full-scale and simulation systems is n in the simulation experiment, to make the simulation experiment have the same physical process as the full-scale experiment, the time scale equal to n and the scale of impulse currents amplitude equal to n^2 can be obtained based on the electromagnetic field theory and the analog criteria [18]. Moreover, the geometrical dimensional scale of our simulation experiment is 10.

A. Test Objects

The simulation experiment is performed in a hemispherical sand pond made of steel (diameter = 5 m and resistivity = 115 Ω·m. Seven typical grounding electrode configurations are illustrated in Figs. 4(a)–(g). The embedded depth of the horizontal grounding electrode in the sand pond is 0.06 m. The grounding electrodes are made of round steel (radius = 0.004 m). The number notation marked on the grounding electrodes is the measurement point, and the distance between the neighboring measurement points is 0.1 m. Impulse currents of 8/20 μs waveshape are injected into the grounding electrodes. The maximum impulse current peak value used in our simulation experiments is 168 A. The scale of impulse currents amplitude between the simulation and full-scale grounding devices is equal to n^2, so the physical process in the simulation experiment under the impulse current with peak value 168 A is equivalent to the full-scale experiment under the impulse current with amplitude of 16.8 kA. A series of measurements on the axial current distribution of the grounding electrodes under lightning currents was performed.

B. Test Circuit and Measurements

Fig. 5 shows the current generation circuit and the measuring circuit arrangement. In the figure, the rated voltages of the transformer T_2 are 0.38/45 kV; the rated current of the high voltage rectifier D is 1A. In our simulation experiment, the capacitance of the charging capacitor bank C is 30 μF, comprised of ten parallel 3 μF capacitors. The waveform adjustable resistance R_0 and inductance L_0 are 6 Ω and 32.97 μH, respectively. The maximum impulse current peak value generated by the impulse current generator is up to 200 kA. The digital storage oscilloscope CRO with a 1.0 GSamples/s sampling rate and 100 MHz bandwidth is used to register the impulse current obtained by the current sensor S. We selected the Rogowski-coil current sensor in our tests. Its major technical performance indices are that the low cutoff frequency is 160 Hz, high cutoff frequency is 4 MHz, and the maximum peak current is 20 kA. To insulate the current sensor from the nearby soil, a layer of epoxy resin with a thickness of 8 mm is poured on the surface of current sensor. To decrease the effect of the current sensor on the flow of leakage current, we select the external diameter and inner diameter as 102 mm and 54 mm, respectively, and the width is 25 mm. E and P are grounding electrodes and the hemispherical sand pond, respectively.

After the 380 V power frequency supply is switched on, voltage regulator T1 regulates the voltage on the high-voltage side of the step-up transformer T2, and then the voltage is

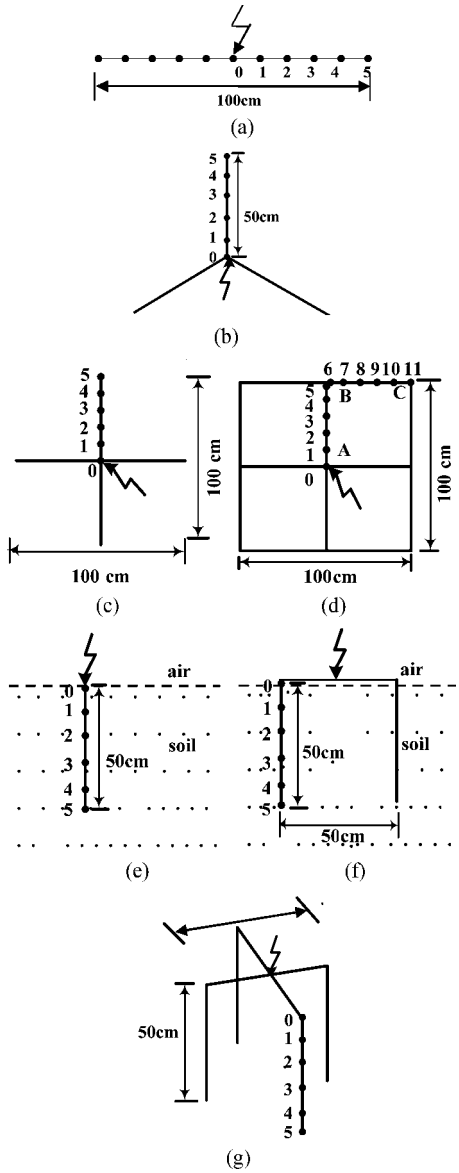

Fig. 4. Configurations of the grounding electrode. (a) Configuration I. (b) Configuration II. (c) Configuration III. (d) Configuration IV. (e) Configuration V. (f) Configuration VI. (g) Configuration VII.

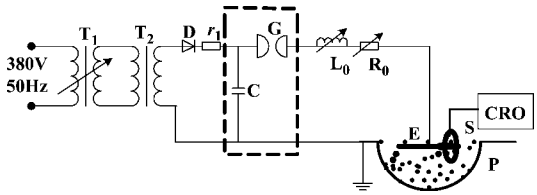

Fig. 5. Wiring diagram of impulse-current test T_1-voltage regulator, T_2-voltage booster, D-silicon stack, r_1-protection water resistance, C-charging capacitor, G- ball gap, L_0-adjustable inductance, R_0-adjustable inductance, CRO-oscilloscope, S-current sensor, E-grounding electrode, P-sand pond.

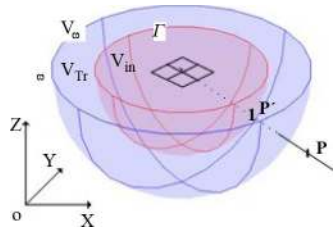

Fig. 6. FEM geometric model of the grounding grid.

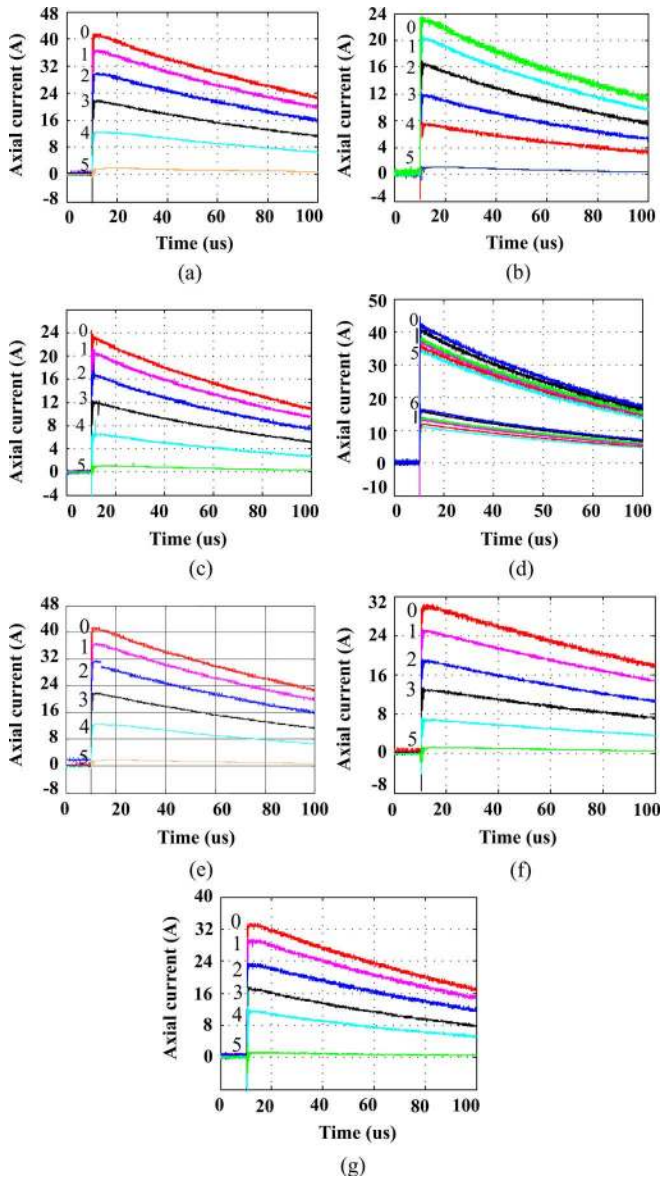

Fig. 7. Axial current curves of the grounding electrode. (a) Configuration I. (b) Configuration II. (c) Configuration III. (d) Configuration IV. (e) Configuration V. (f) Configuration VI. (g) Configuration VII.

rectified by silicon diode stack D. When capacitor bank C is charged for a period of time, the capacitor C is discharged by the ignition pulse triggering the ball gap G, forming an 8/20 μs impulse current injected into the grounding electrode E in the sand pond P. In the measurement circuit, the current sensor S is placed at the measurement point of the electrode and the axis of the sensor and the conductor should be coinciding. The digital oscilloscope CRO, which is connected to the sensor through a coaxial cable, is used to register the axial current in the conductor at the measured point where the impulse current dissipates into the earth. To reduce accidental measurement errors, the measurements of every configuration at each measurement point are repeated three times under the same test conditions.

V. Model Validation

With the intention to verify the application capability and the reliability of the proposed methodology, the computer modeling has been performed on the grounding electrodes shown in Fig. 4 and the single vertically grounding rod in [5]. The proposed numerical scheme is validated by comparing the calculated results with measurements and simulations results found in [5].

A. Comparison of Experimental and Calculated Results

In Fig. 6, the FEM geometric model of the grounding grid is sketched, the hemispherical surface Γ is the interface of the internal hemisphere $V_{\rm in}$ and the external infinite space V_{∞}. The hemispherical shell $V_{\rm tr}$ is the transformation region transformed from the external infinite domain through the spatial transformation T. The spatial transformation T is introduced to overcome the contradiction between the infinite domain and the finite computer storage; and it is a single-valued and reversible transformation that translates point P in V_{∞} to point P' in $V_{\rm tr}$[24].

To facilitate analysis, I (n) is defined as the average value of the axial current crest value of the three repetitive tests at the measurement point n; I (0) denotes the average value of the axial current crest value at the first measurement point (0) of the electrode conductor branches near the current input point. Furthermore, [I(n)-I(n-1)]/I(0) is the relative leakage current when axial current arrives at the crest, reflecting the average dispersal capacity of the electrode conductor segment between measurement points n-1 and n.

According to the injection locations shown in Fig. 4, impulse currents are injected into the grounding electrode configurations, respectively.Figs. 7(a)–7(g) present the measured axial current curves of the grounding electrode at the measurement points. The number marked beside the curve stand for the measurement points corresponding to the current curves. Fig. 8 presents the computed results of total current density distribution on a horizontal observation surface (for the horizontal grounding electrode) or a vertical observation surface (for the vertical grounding electrode) at peak of injection current. The distance between the observation surface and the grounding electrode is 0.02 m.

From the axial current curves and the current density distribution profile at the peak of impulse current, the relative leakage current $[\mathrm{I(n)} - \mathrm{I(n-1)}]/\mathrm{I(0)}$ distribution along the seven grounding electrode configurations at the peak of the impulse current can be obtained as shown in Fig. 9. According to Figs. 9(a)–(h), these comparisons between experimental and calculated results show the agreement in the relative leakage current distribution of the seven typical grounding electrode configurations. It is hence concluded that the model proposed can successfully be applied to describe, within acceptable accuracy, the dynamic electromagnetic and current density field in the soil. The accurate knowledge of electromagnetic and current density field behavior is a major step forward, as grounding systems can now be represented in a dynamic manner with more information. It is believed that such a dynamic representation of the grounding system, in place of the surge resistance used before, will certainly be useful for the optimization design of grounding systems and electromagnetic compatibility of the power system.

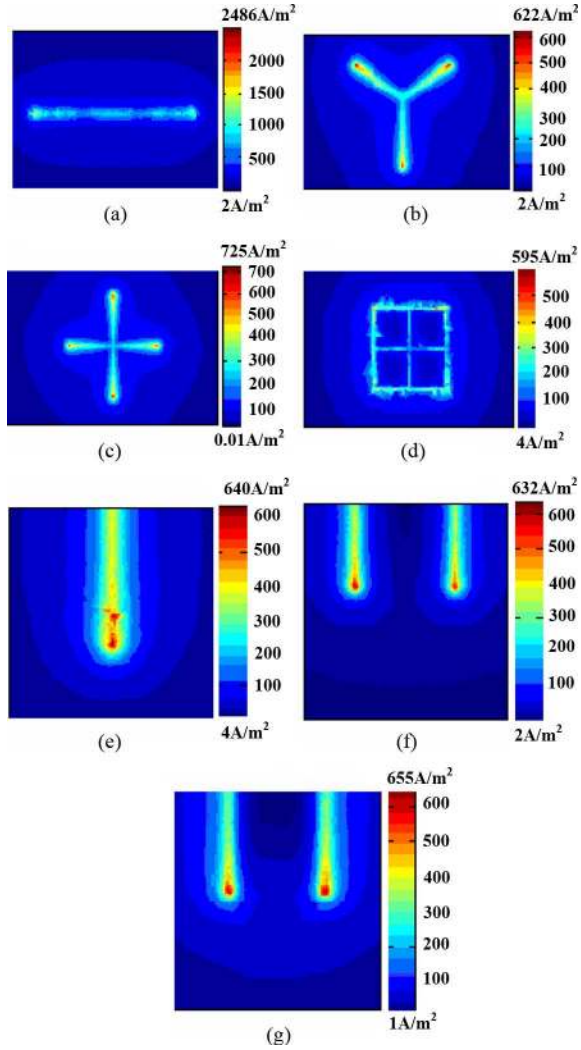

Fig. 8. Total current density distribution on the observation surface at peak of injection current. (a) Configuration I. (b) Configuration II. (c) Configuration III. (d) Configuration IV. (e) Configuration V. (f) Configuration VI. (g) Configuration VII.

B. Single Vertical Rod Simulation

According to [5], a single steel rod with a length of 1 m and radius of 25 mm was analyzed. The grounding rod was placed vertically from the earth surface into the uniform soil with the resistivity of 43.5 Ω·m. To estimate the influence of the soil ionization on the behavior of grounding systems excited by high magnitude currents, a FEM analysis of grounding resistance and GPR (grounding potential rise) at various injected current magnitudes $I_{\rm max}$ was carried out. $I_{\rm max}$ is varied from 5.2 to 30.8 kA. Table I summarizes the computed values, obtained from model in[5] COMP) and from our suggested model FEM), as well as the results of measurements (MEA) performed on a vertically buried steel rod in [5].

As was to be expected, the grounding resistance decreases as the current increase from 5.2 to 30.8 kA. This reduction justifies the necessity of including the simulation of soil breakdown in the engineered analysis of grounding systems. The good agreement between the measurements and the numerical results shows the validity of our proposed method and permits

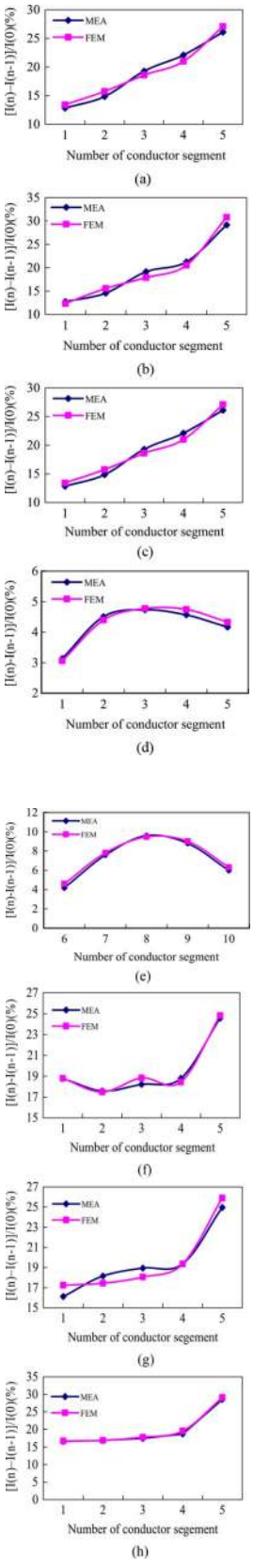

Fig. 9. Relative leakage current of the horizontal grounding electrodes at peak of injection current. (a) Configuration I. (b) Configuration II. (c) Configuration III. (d) Conductor segment AB of configuration IV. (e) Conductor segment BC of configuration IV. (f) and (g) Configuration VI and configuration V. (h) Configuration VII.

TABLE I
MEASURED AND COMPUTED RESULTS FOR THE VERTICAL ROD

Imax (kA)	GPR(kV)			R(Ω)		
	MEA	*COMP*	*FEM*	*MEA*	*COMP*	*FEM*
5.2	92	95.1	91.1	17.7	18.3	17.5
10.5	137	147.3	140.2	13	14	13.4
21.4	200	212.7	201.5	9.3	9.9	9.4
27.2	230	236	229	8.5	8.7	8.4
30.8	248	248.3	247.6	8.1	8.1	8

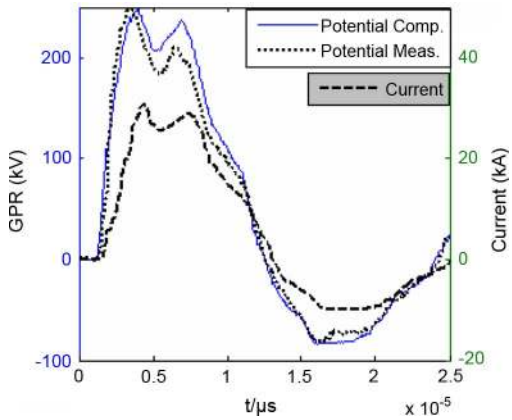

Fig. 10. Waveshapes of the injected current, the measured and computed earth potential for the vertical rod.

confirming that our model simulates the soil ionization phenomenon in a quite accurate way.

Fig. 10 shows the waveform of injected current, whose amplitude ranges the level of 30.8 kA, provoking soil ionization. The rise time of the injected impulse current was constant and equal to 2.5 μs for all test conditions. In Fig. 10, the waveshapes of the earth potential are shown with reference to the measurements and to the computations. The waveshapes of earth potentials (measured and computed) show a quite similar trend. The different rise time is probably caused by measurement errors due to coupling effects. It is believed that such a dynamic representation of grounding system will certainly reduce the uncertainties in this very important parameter for back flashover calculation.

Fig. 11 shows the transient current density distribution in the soil when the impulse current with the amplitude of 30.8 kA is dissipated into the soil. From it, we can observe: 1) Fig. 14(a) shown that at the initial period of the impulse current, because the transient current value is relatively small, the leakage current along the grounding rod appears uniform. The end effect of the leakage current along the grounding rod is not distinct. 2) Figs. 14(b)–(d) show that when the impulse current is larger, the end effect is more obvious. If the current is large enough, it evokes the soil ionization phenomenon. The soil resistivity decrease induced by the ionization phenomenon will enlarge the leakage current which disperses from the end of the grounding electrode.

VI. ANALYSIS AND DISCUSSION

With the intension of optimizing the grounding system and developing the installations safety, we analyzed the impulse dis-

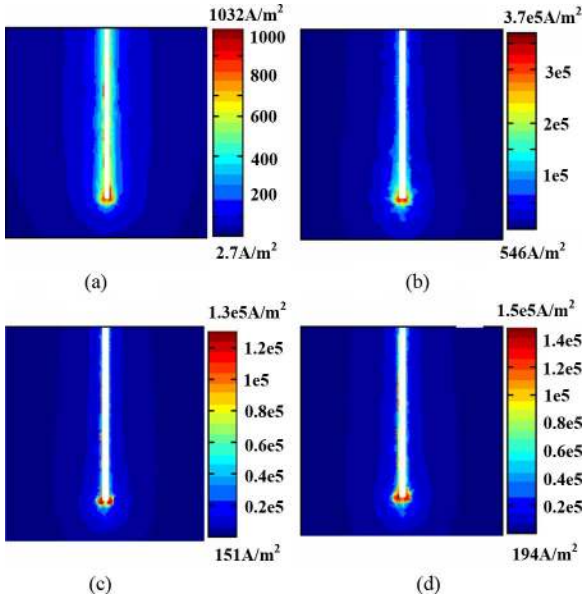

Fig. 11. Dynamic distribution of leakage current on the vertical grounding rod. (a) t = 1 μs. (b) t = 4 μs. (c) t = 12 μs. (d) t = 15 μs.

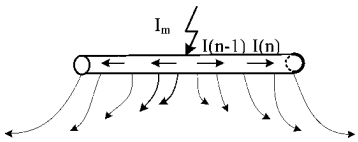

Fig. 12. Sketch of shielding effect on a horizontal grounding electrode.

persal regularity of the typical grounding system and discussed the effect of ionization on human and installations.

A. *Impulse Current Dispersal Regularity*

As shown in Figs. 8(a) and 9(a), when the impulse current is applied to the horizontal grounding electrode configuration I at the middle point, the relative leakage current increases as the distance from the current injection point increases. When impulse current is injected into the electrode, leakage current on the interface of the soil and the conductor is considered perpendicular to the conductor surface and parallel to each other, as shown in Fig. 12. The leakage current produces time-varying magnetic field in the soil, and the induced current caused by the time-varying magnetic field flowing to the opposite direction of the leakage current appears. According to the relative position of the conductor segment in the grounding electrode, the induced current along the grounding electrode is nonuniform. So the leakage currents along the grounding electrode comprised by the initial leakage current and the induced current are also nonuniform. The leakage current at the two ends are more than that at the segment near the middle injection point. The increase in leakage current at the last segments at the end of the rod may be due to an "end effect" [25].

From the leakage current distribution diagrams of grounding electrode configurations I II and III in Fig. 9, the leakage current distribution trends are similar. However, the shielding effect is more remarkable when the impulse currents are injected into the star-shaped and cross-shaped grounding electrode at the central point. The differences in leakage current between the head part

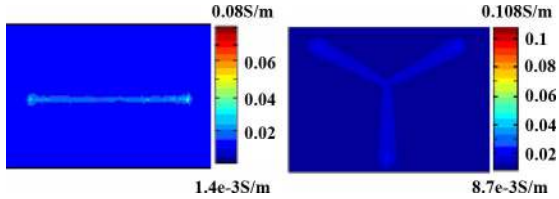

Fig. 13. Conductivity distribution in the soil.

of each conductor branch and the terminal part are greater than that of the single horizontal electrode. More conductor branches near the injection point result in a more uneven leakage current distribution.

Based on the leakage current distribution diagram of the grounding grid in Fig. 9(d) and (e), the total leakage current of conductor segment AB is smaller than that of BC. It is because the inner conductor segment AB is surrounded by the outer conductor segments, the shielding effect on AB caused by the next and the outer conductor segment is larger. Moreover, the leakage distribution along the conductor AB or BC is nonuniform. The leakage current is larger at the middle and is smaller at the two ends of the conductor segment. Hence, the leakage current along the conductor must not be considered uniform in the simulation modeling, and it is necessary to consider the shielding effect of the grounding electrode in the economical design of the grounding system.

We compare the impulse current dispersal regularly of the three vertical grounding system, and find that the leakage current along the conductor is uneven. Moreover, it gradually increases with ground depth. When the number of conductor branches connected in parallel is increased from one to four, the nonuniformity of the leakage current along the branches becomes more serious. The results imply that the shielding effect plays an important role when grounding electrodes are constructed by a few parallel conductor branches.

B. *Ionization Phenomenon and It's Effect On Grounding System Characteristics*

To illustrate the ionization phenomenon in the dispersal process of impulse current, as an example, the conductivity distribution and electrical field intensity at the time step of 8 μs on the observation surface are presented in Figs. 13 and 14. The distance between the observation surface and the single horizontal electrode and the star-shaped electrode is 1 cm. In accordance with the soil ionization theory, when the electrical field intensity caused by the discharge of the impulse current exceeds a certain value, the resistivity of the soil decreases according to the relationship between soil resistivity and the electrical field. In the conductivity profiles of the single horizontal and star-shaped electrode, the increase of conductivity in the soil surrounding the grounding electrode coincides with the ionization theory. According to (1), the electrical field intensity in the ionization soil region decreases as well. This can be observed in Fig. 14.

Good agreement between theory and the numerical results on the ionization phenomenon confirms that the model simulates the physical phenomenon in an accurate way both for the design of the grounding system and for accurate investigations on the

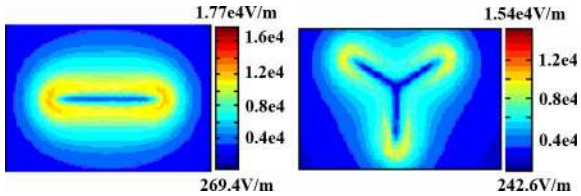

Fig. 14. Electrical field distribution in the soil.

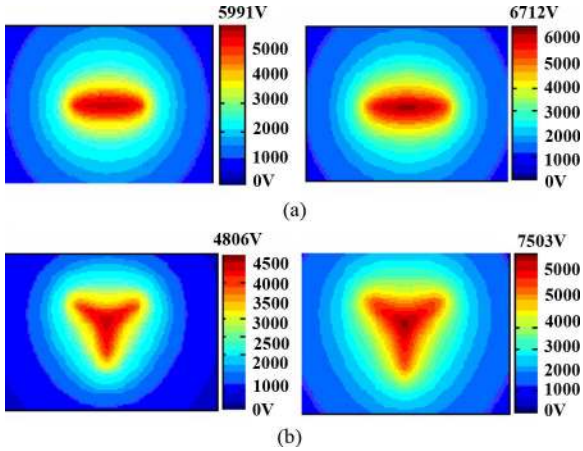

Fig. 15. Potential distribution with and without soil ionization. (a) Potential distribution of the single electrode with and without ionization. (b) Potential distribution of the star-shaped electrode with and without ionization.

disturbance level induced, inside of the protected volume, by a complete lightning protection system struck by a thunderbolt.

The soil ionization basically converts the affected portion of the soil from an insulator to a conductor and is simply equivalent to an increase in the size of the electrode. Hence the grounding potential rise encountered during the discharge is less than that of the condition without soil ionization. As seen from the potential distribution profile in Fig. 15, the consideration of the soil ionization enables a reduction in potential peak amplitudes, with an average decrease of about 12% and 41% for the single horizontal electrode and the star-shaped electrode, respectively.

To analyze the effect of ionization on the characteristics of the grounding system in detail, the ground potential rise and the step voltage of the single vertical electrode are reported in Fig. 16. The image shows a reduction in ground potential distribution. This can be helpful in case of direct touch voltage; however, a complete study is required to consider step voltage. The ionization of the soil surrounding the electrode modifies the distribution of electric field in the soil, as shown in Fig. 14, the ionization of the soil virtually pushes the domain with a larger electric field from the surface of electrode to a more remote domain, which is the considered step path. So the step voltage around the grounding system under the impulse current does not decrease as the ground potential.

In other words, the numerical method based on electromagnetic field theory can compute the spatial electric field at every time step, hence, the instantaneous geometries of the ionized region are automatically built according to the actual spatial electric field at every time step. No predefined location and shape of soil ionized zones need to be introduced. Moreover, the time

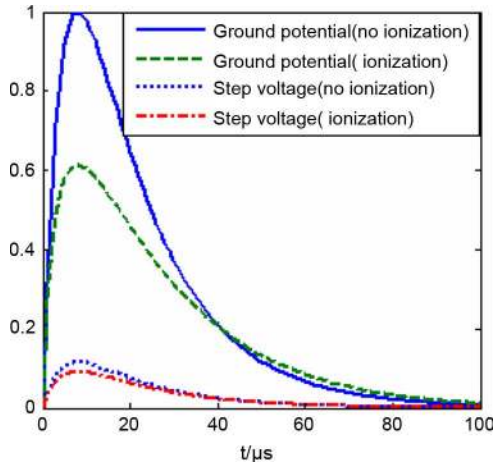

Fig. 16. Step voltage of the point 60 cm away from the rod between two points 60 cm apart referred to the nonionized potential to remote ground.

variable resistivity model is built from an examination of the observed experimental voltage and current time profiles. Thermal, ionization, and sparking effects are included in the adopted time variable resistivity model.

The proposed methodology is the primary investigation on the impulse characteristic of grounding system considering the transient ionization phenomenon in the soil. Actually, the time dependent nonlinear behavior related to soil ionization and the frequency-dependent electromagnetic effects related to fast rise-time current pulses will influence the dynamic performance of grounding electrodes during lightning discharge. It should be noted that for soils, σ and ε are frequency-dependent. The frequency domain electromagnetic transients program proposed in the literature [11] decouple the transient impulse current into a succession of step functions, then compute the response of grounding system under the step function current in the frequency domain, in which the frequency dependency of soil parameter is included. The investigation conducted by Salari in [11] is important for the improvement of our electromagnetic modeling in the time domain. In order to incorporate the frequency dependency characteristic of soil electric parameter in our modeling and obtain the more accurate electromagnetic field distribution in the soil, we will improve our methodology through decoupling the transient impulse current, referring to [11], and adding the Fourier transforms into the finite element method to compute the frequency domain response of the grounding system under the step function based on the proposed time domain electromagnetic field modeling.

VII. Conclusion

In this paper, a numerical scheme that combines the FEM with FDTD is proposed to analyze the soil ionization and the dispersal regularity of the grounding electrodes during the soil breakdown that can take place when a surge current has to be drained. The space-time variable soil resistivity approach is embedded in the FEM scheme to simulate the nonlinear effect of soil ionization processes. The paper demonstrates that no guess of a predefined location and shape of ionized zones of the soil need to be introduced. Thus, the soil zones may or may not be

ionized depending on the local electric field intensity. Based on the principle of dimensional similarity, this paper makes simulation experimental investigations on the impulse-current distribution of grounding electrodes with various structures. The proposed numerical scheme is validated by comparing experimental results with computed results. A satisfactory agreement is reached.

The impulse current dispersal regularity of grounding electrodes and the soil ionization process are investigated in detail based on measurement and simulation computation results. The impulse-current dispersal regularity of grounding electrodes with various structures in homogeneous soil is obtained.

- For horizontal grounding electrodes with branch conductors and vertical grounding electrodes constructed by a few parallel conductor branches, the leakage currents along the branches increase with the distance from the current feed point; more conductors near the injection point result in a more uneven leakage current distribution.
- For the simple grounding grid, the leakage currents of the conductor segments in different positions are different. The leakage currents along the same conductor segment are nonuniform as well.

The shielding effect between grounding conductor segments plays a significant role in the discharge of impulse current. On the other hand, the decrease in soil resistivity caused by the ionization phenomenon can be helpful in case of direct touch voltage, but the ionization of the soil surrounding the electrode modifies the distribution of current in the soil. The ionization of the soil virtually approaches the injecting surface of the electrode to the considered step path; the effect is increasing the step voltage. Therefore, the ionization phenomenon and the nonuniform leakage distribution along the grounding conductor should always be taken into account for the economical and accurate design, as well as for the calculation, of the grounding system.

REFERENCES

[1] *IEEE Standard Dictionary of Electrical and Electronics Terms*, IEEE Std. 100–1992, Jan. 1993.

[2] B. R. Gupta and B. Thapar, "Impulse impedance of grounding grids," *IEEE Trans. Power App. Syst.*, vol. PAS-99, no. 6, pp. 2357–2362, Nov. 1980.

[3] A. Geri, "Behavior of grounding systems excited by high impulse currents: the model and its validation," *IEEE Trans. Power Del.*, vol. 14, no. 3, pp. 1008–1017, Jul. 1999.

[4] A. F. Otero, J. Cidras, and J. L. Alamo, "Frequency dependent grounding system calculation by means of a conventional nodal analysis technique," *IEEE Trans. Power Del.*, vol. 14, no. 3, pp. 873–878, Jul. 1999.

[5] A. Geri, G. M. Veca, E. Garbagnati, and G. Sartorio, "Non-linear behavior of ground electrodes under lightning surge currents: computer modeling and comparison with experimental results," *IEEE Trans. Magn.*, vol. 28, no. 2, pp. 1442–1445, Mar. 1992.

[6] B. Zhang, X. Cui, Z. B. Zhao, and L. Li, "Analysis of grounding grids at large scale substations in frequency domain," in *Proc. CSEE*, Sep. 2002, vol. 22, pp. 59–63.

[7] W. X. Sima, X. L. Li, and T. Yuan, "Analysis of grounding grid impulse characteristics in frequency domain in consideration of soil non-linear characteristic," in *Proc. CSEE*, Jun. 2009, vol. 29, pp. 127–132.

[8] L. Qi, X. Cui, Z. B. Zhao, and H. Q. Li, "Grounding performance analysis of the substation grounding grids by finite element method in frequency domain," *IEEE Trans. Magn.*, vol. 43, no. 4, pp. 1181–1184, Apr. 2007.

[9] L. Grcev, "Impulse efficiency of ground electrodes," *IEEE. Trans. Power Del.*, vol. 24, no. 1, pp. 441–451, Jan. 2009.

[10] L. Grcev, "Time and frequency dependent lightning surge characteristics of grounding electrodes," *IEEE. Trans. Power Del.*, vol. 24, no. 4, pp. 2186–2197, Oct. 2009.

[11] J. C. Salari and C. Portela, "Grounding systems modeling including soil ionization," *IEEE Trans. Power Del.*, vol. 23, no. 4, pp. 1939–1945, Oct. 2008.

[12] J. P. Wang, A. C. Liew, and M. Darveniza, "Extension of dynamic model of impulse behavior of concentrated grounds at high currents," *IEEE Trans. Power Del.*, vol. 20, no. 3, pp. 2160–2166, Jul. 2005.

[13] M. Ramamoorty, M. M. B. Narayanan, S. Parameswaran, and D. Mukhedkar, "Transient performances of grounding grids," *IEEE Trans. Power Del.*, vol. 4, no. 4, pp. 2053–2059, Oct. 1989.

[14] Z. StojkoviC, M. S. Savid, J. M. Nahman, D. Salamon, and B. Bukorovic, "Sensitivity analysis of experimentally determined grounding grid impulse characteristics," *IEEE Trans. Power Del.*, vol. 13, no. 4, pp. 1136–1142, Oct. 1998.

[15] S. Sekioka, T. Sonoda, and A. Ametani, "Experimental study of current-dependent grounding resistance of rod electrode," *IEEE Trans. Power Del.*, vol. 20, no. 2, pt. 2, pp. 1569–1566, Apr. 2005.

[16] C. W. Yang, W. X. Sima, T. Yuan, and Q. Yang, "Experimental analysis on shielding effect of the grounding electrodes under impulse current," *High Voltage Eng.*, vol. 34, pp. 2609–2615, Dec. 2008.

[17] B. S. Wang, W. F. Wan, Y. J. Yang, and S. S. Ma, "Impulse current distribution characteristic of long grounding rod/pole," *High Voltage Eng.*, vol. 21, pp. 70–73, Mar. 1995.

[18] J. L. He, R. Zeng, Y. P. Tu, J. Zou, S. M. Chen, and Z. C. Guan, "Laboratory investigation of impulse characteristics of transmission tower grounding devices," *IEEE Trans. Power Del.*, vol. 18, no. 3, pp. 994–1001, Jul. 2003.

[19] J. L. He and R. Zeng, *Grounding technologies for power system*. Beijing, China: Publisher of Science, 2007.

[20] M. Laboda and Z. Pochanke, "Experimental study of electric properties of soil with impulse current injections," in *Proc. 18th ICLP Munich*, Munich, Germany, 1985, pp. 191–198.

[21] Y. Q. Liu, N. Theethayi, R. M. Gonzalez, and R. Thottappillil, "The residual resistivity in soil ionization region around grounding system for different experimental results," in *Proc. IEEE Int. Symp. Electromagn. Compat.*, 2003, pp. 794–799.

[22] A. M. Mousa, "The soil ionization gradient associated with discharge of high currents into concentrated electrodes," *IEEE Trans. Power Del.*, vol. 9, no. 3, pp. 1669–1677, Jul. 1994.

[23] Y. Q. Gao, J. L. He, J. Zou, R. Zeng, and X. D. Liang, "Fractal simulation of soil breakdown under lightning current," *J. Electrostat.*, vol. 61, pp. 197–207, Feb. 2004.

[24] A. Stochniol, "A general transformation for open boundary finite element method for electromagnetic problems," *IEEE Trans. Magn.*, vol. 28, no. 2, pp. 1679–1681, Mar. 1992.

[25] X. L. Chen, Y. G. Liu, and Y. Huang, *Grounding*. Chongqing, China: Chongqing Univ. Press, 2002.

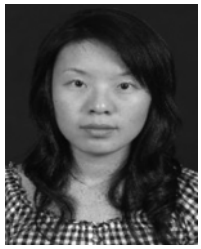

Jingli Li (M'11) was born in Henan Province, China, on October 22, 1983. She received the B.S. degree in electrical engineering from Zhengzhou University, Zhengzhou, China, in 2005 and is currently pursuing the Ph.D degree in electrical engineering at Chongqing University, Chongqing, China.

Her research interests include overvoltage protection and grounding technology in power systems.

Tao Yuan received the B.S. degree from Sichuan Polytechnic Institute, China, in 1999, and the M.Sc. and Ph.D. degrees from Chongqing University, Chonqing, China, in 2001 and 2010, respectively.

Currently, he is a Lecturer at Chongqing University. His research interests include overvoltage protection and grounding technology in power systems.

Qing Yang (M'11) received the B.S. degree from North China Electrical Power University, Baoding, China, in 2002 and the Ph.D. degree in electrical engineering from Chongqing University, Chonqing, China, in 2006.

Currently, he is an Associate Professor in the State Key Laboratory of Power Transmission Equipment and System Security and New Technology, Chongqing University. His research interests include outdoor insulation in complex ambient conditions and electric-field calculations. He is the author and coauthor of more than 30 journal and international conference papers.

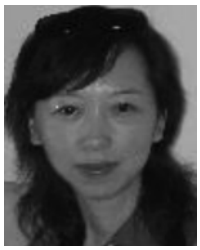

Wenxia Sima was born in Henan Province, China, on July 13, 1965. She received the Ph.D. degree from Chongqing University, Chongqing, China, in 1994.

Her employment experience includes the College of Electrical Engineering, Chonging University. Her fields of interest include high-voltage outdoor insulation and overvoltage protection.

Caixin Sun received the B.S. degree in electrical engineering from Chongqing University, Chonqing, China, in 1969.

Currently, he is Professor at Chongqing University, leading the research group on high-voltage engineering. His research interest is high-voltage engineering, especially online detection of insulation condition and insulation fault diagnosis for high-voltage equipment, discharge mechanism of outdoor insulation in complicated environments, and high-voltage techniques applied to biomedicine. He is an author and coauthor of many publications.

Prof. Sun is a member of the Chinese Academy of Engineering and Director of the Electrical Power Engineering Committee of the National Science Foundation of China.

Markus Zahn (LF'12) received the B.S.E.E., M.S.E.E., electrical engineer, and D.Sc. degrees in electrical engineering from the Massachusetts Institute of Technology (MIT), Cambridge, , in 1968, 1968, 1969, and 1970, respectively.

He then joined the Department of Electrical Engineering, University of Florida, Gainesville, until 1980 when he returned to MIT, where he is now Professor of Electrical Engineering working in the Research Laboratory of Electronics, Laboratory for Electromagnetic and Electronic Systems and the High Voltage Research Laboratory. He is also the Director of the MIT Course VI-A EECS Internship Program, a cooperative work/study program with industry. He is the author of *Electromagnetic Field Theory: A Problem Solving Approach* (now out of print) but is working on a new reference book with a complete collection of solved electromagnetism problems. He has also co-developed a set of educational videotapes on demonstrations of electromagnetic fields and energy for the enriched teaching of electromagnetism. He has received numerous excellence in teaching awards at the University of Florida and MIT. His primary research areas are ferrohydrodynamics and electrohydrodynamics for microfluidic and biomedical applications, nanoparticle technology for improved high-voltage performance of electric power apparatus, modeling of electrical streamer initiation and propagation leading to electrical breakdown, Kerr electro-optic field and space charge mapping measurements in high-voltage stressed materials, and for the development of model-based interdigital dielectrometry and magnetometry sensors for measurement of dielectric permittivity, electrical conductivity, and magnetic permeability with applications to nondestructive testing and evaluation measurements and for the identification of metal and low-metal content dielectric landmines and unexploded ordnance. He is a Co-Inventor on 19 patents. He has contributed to about 10 book and encyclopedia chapters, about 115 journal publications, and about 175 conference papers.

Prof. Zahn was a Distinguished Visiting Fellow of the Royal Academy of Engineering at the University of Manchester, Manchester, U.K.; the 1998 J.B. Whitehead Memorial Lecturer; and was the first James R. Melcher Memorial Lecturer in 2003. He is an Associate Editor of the IEEE TRANSACTIONS ON DIELECTRICS AND ELECTRICAL INSULATION, is on the International Scientific Committee on Magnetic Fluids, and has received a Certificate of Achievement for completion of the "Deminers Orientation Course" at the Night Vision and Electronic Sensors Directorate Countermine Division, Ft. Belvoir, VA.